

An effective transformer less 7 level inverter with optimized PID and buck boost controller for grid-connected PV systems

B. Mohan Rao¹, Md. Haseeb Khan², B. Mangu¹

¹Department of Electrical Engineering, University College of Engineering (A), Osmania University, Hyderabad, India

²Muffakham Jah College of Engineering and Technology, Osmania University, Hyderabad, India

Article Info

Article history:

Received May 15, 2024

Revised Aug 10, 2024

Accepted Aug 15, 2024

Keywords:

Multi-level inverter

Power quality

Total harmonic distortion

Transformer less

Trapezoidal PWM

ABSTRACT

This research paper presents an effective transformer-less seven-level inverter with an optimized proportional-integral-derivative (PID) controller and buck-boost controller for grid-connected photovoltaic (PV) systems. The proposed model aims to achieve optimum power quality (PQ) in a hybrid power system integrating battery and PV. This is accomplished by utilizing a unified power quality conditioner (UPQC-PQ) with active and reactive power is developed, utilizing a hybrid metaheuristic algorithm named the honey badger algorithm (HBA) along with the equilibrium optimization algorithm (EOA), referred to as the honey badger equilibrium optimization (HBEO) algorithm. The PID controller in the proposed model is optimized using the HBEO algorithm, resulting in a highly efficient hybrid renewable energy system. By incorporating a 7-level multilevel inverter model with minimal switch usage (only 5 switches instead of 12), the proposed model ensures minimal switching losses. The proposed model is implemented and verified through the MATLAB/Simulink platform.

This is an open-access article under the [CC BY-SA](#) license.



Corresponding Author:

B. Mohan Rao

Department of Electrical Engineering, University College of Engineering (A), Osmania University

Hyderabad, Telangana, India

Email: bodamohan1@osmania.ac.in, bodamohan1@gmail.com

1. INTRODUCTION

Renewable energy sources are becoming more and more necessary for the production of power for both industrial and household uses [1]. PV systems are becoming more and more popular as renewable energy sources these days since they are clean, quiet, environmentally friendly, and require fewer upkeep tasks. The sporadic variability of sources of renewable energy, however, presents several complications for the utility grid's power quality [2]. During the peak of PV generation, reverse power flow may cause a sudden voltage surge [3]. For many years, photovoltaic (PV) systems have been using PV as a type of renewable energy source. The affordable and efficient functioning of renewable energy absorption is largely dependent on power electronics equipment, particularly for inexpensive DC/AC PV inverters [1], [4], [5]. Transformer-less grid-connected photovoltaic inverters can be connected straight to the electrical grid and do not require a transformer [2], [3], [6]-[8]. Inverters of these types are less expensive, lighter, more cost-effective, and have reduced switching losses. There are a few shortcomings with these inverters, though. Common-mode voltage variations brought on by voltage variations in the PV cell's stray capacitors result in additional leakage current flow [9]-[25].

This work contributes to the reduction of total harmonic distortion (THD) and enhancement of power quality by supporting a seven-level inverter topology with five switches. In order to cut down on complexity, expense, and switching losses, a seven-level inverter with only five switches used is proposed. To increase the effectiveness and performance of the proportional-integral-derivative (PID) controller, a hybrid metaheuristic

honey badger equilibrium optimization (HBEO) algorithm is utilized by combining the equilibrium optimization algorithm (EOA) and the honey badger algorithm (HBA).

To use trapezoidal pulse width modulation (PWM) to produce voltage regularization and reduce THD of the output voltage. To develop a unified power quality conditioner with active and reactive power (UPQC-PQ) to improve power quality (PQ) in a hybrid power system. A consistent and dependable grid-connected operation is ensured by the UPQC-PQ, which is built to reduce voltage fluctuations, and other PQ concerns. To lower switching losses and improve the overall system efficiency by using a 7-level multilevel inverter architecture with only 5 switches instead of 12. The system has more energy- and cost-efficient as a result of the fewer switches, which also results in lower power losses.

The difficulties posed by transformer less inverters' decreased switching, especially when it comes to grid-connected photovoltaic (PV) systems. Transformer less inverters have benefits like low cost, compact size, and great efficiency, but they also have problems with earth leakage current, which poses electrical and security risks. Numerous studies [17], [21], [22] have suggested approaches to deal with these issues, including the development of creative inverter concepts, fault-tolerant topologies, and control strategies. To guarantee dependable and effective functioning, more research and optimization of these solutions are necessary, particularly when non-linear loads and fluctuating grid circumstances are present. To determine the best method for broad implementation in PV grid-connected systems, a comparison of various inverter topologies, control schemes, fault tolerance techniques and using energy-storage combination structures and sophisticated control methods such as fuzzy logic-based switching, model predictive control (MPC), and selective harmonic elimination pulse width modulation (SHE-PWM) is also necessary. To overcome the above limitations here comes an effective transformer less 7-level inverter with optimized PID and buck boost controller for grid connected PV systems which is implemented in this investigation. The purpose of this research is to improve transformer less inverter safety, dependability, and efficiency.

2. METHOD

Transformer less inverters frequently have switching losses, which can lead to difficulties with heat dissipation. Inaccurate tuning may lead to issues including harmonic distortion, voltage instability, or poor power transmission. Any deviations or issues with non-compliance could hinder the inverter design's implementation and widespread acceptance. To overcome these challenges, the suggested model pursues integrating PV and batteries into a hybrid power system while achieving optimal power quality. Trapezoidal PWM is used to minimize THD, while a 7-level inverter with 5 switches reduces switching losses. The UPQC-PQ is developed using the hybrid metaheuristic algorithm, HBEO, which optimizes the PID controller for a highly efficient hybrid renewable energy system. Trapezoidal PWM is employed for voltage regularization, minimizing THD. The model also incorporates a buck-boost controller to adjust the voltage level, increasing or decreasing it based on the PV input voltage, while a 7-level multilevel inverter with minimal switches (5 instead of 12) ensures minimal switching loss. The proposed model is implemented and verified using the MATLAB/Simulink platform under various temperature and solar irradiance conditions, compared with existing techniques like PSO, GA, and MO. The block diagram for the proposed model is shown in Figure 1.

2.1. Modeling of PV

A few parallel-connected strings of PV modules make up the PV model. In addition, each string has a series PV module to meet the necessary power, voltage, and current ratings. A current source linked in parallel with a forward diode, a series-connected resistance, and a parallel resistance make up the design of the single-diode equivalent circuit. The output current of a PV cell is calculated using Kirchhoff's current law as shown in (1)-(4).

$$I_{pv} = I_{ph} - I_{d1} - I_{sh} \quad (1)$$

$$I_d = I_{sd} \cdot \left\{ \exp \left[\frac{q \cdot (V_L + R_s \cdot I_L)}{nKT} \right] - 1 \right\} \quad (2)$$

$$I_{sh} = \frac{V_L + R_s \cdot I_L}{R_{sh}} \quad (3)$$

$$I_l = I_{ph} - I_{sd} \cdot \left\{ \exp \left[\frac{q \cdot (V_L + R_s \cdot I_L)}{nKT} \right] - 1 \right\} - \frac{V_L + R_s \cdot I_L}{R_{sh}} \quad (4)$$

Here, I_l , I_{ph} , I_d , and I_{sh} are the output, photo-generated, diode, and shunt resistor current respectively. The diode current is given by Shockley's equation. R_s and R_{sh} are the series and shunt resistors respectively. V_L is the load voltage, n is the diode ideality factor, k is the Boltzmann constant, T is the Kelvin temperature of the battery, and q is the charge of the electron.

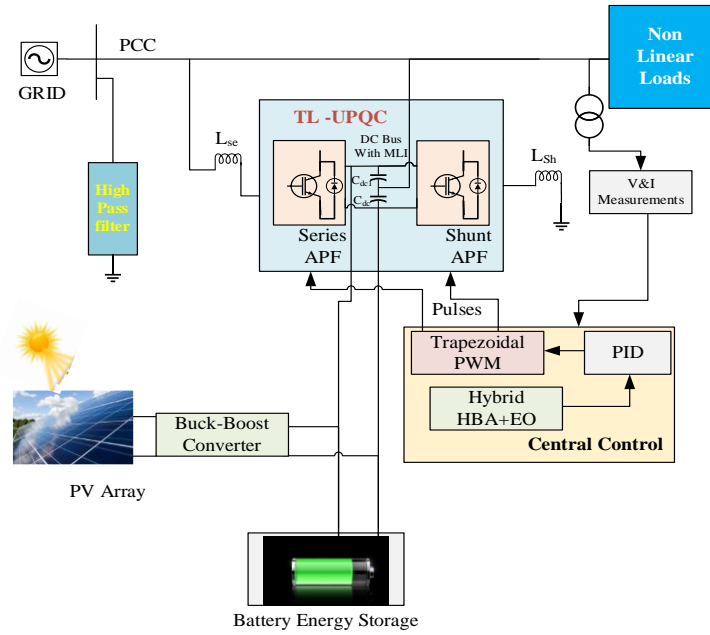


Figure 1. Block diagram of the proposed model

2.2. Buck-boost converter

The buck-boost converter employs trapezoidal PWM to regulate the output voltage. By controlling the gate of the MOSFET switch, the circuit alters the energy transfer between the inductor and the output capacitor indirectly. Notably, the inductor and capacitor are arranged in parallel, acting as a second-order low-pass filter to efficiently reduce the voltage ripple at the output.

In a circuit utilizing an inverting converter topology, the measured output voltage V_{out} across the load exhibits a reversed polarity compared to the input voltage V_{in} . This phenomenon arises because of the way the inductor discharges charge in a buck-boost converter, the V_{out} across the load is defined as (5).

$$V_{out} = -\frac{D}{1-D} V_{in} \quad (5)$$

Here, V_{in} is the input voltage and duty cycle D of the switching transistor. In the boost mode of the buck-boost converter, the duty ratio D is greater than in buck mode. Boost mode has a longer on-state for the switch, allowing more energy to be stored in the inductor before transferring it to the capacitor. This increase in energy leads to a higher output voltage.

In the circuit, the MOSFET switch and diode control the flow of charge. When the MOSFET switch is on, current flows to the inductor, while the diode prevents current from reaching the output. The inductor stores energy as a magnetic field. When the MOSFET switch is off, the diode allows current to flow from the inductor to the rest of the circuit, reversing the inductor's polarity, and resulting in an induced voltage at the output. This process facilitates the transfer of energy to the output and contributes to the converter's functionality. The change in capacitor voltage v_c is given by (7).

$$\frac{di_L}{dt} = \frac{V_{in}}{L} - i_L \frac{R_{on} + r_L}{L} \quad (6)$$

$$\frac{dv_c}{dt} = -\frac{v_c}{RC} \quad (7)$$

2.3. Battery

A battery is typically made up of one or more electrochemical cells connected in parallel or series to produce the required nominal voltage and capacity. The battery energy storage (BES) operates in charge and discharge modes, providing backup power to address short-interval demands not met by PV systems. It aims to maintain a stable DC bus voltage, reducing voltage ripple in the capacitor. Battery models fall into different categories, with the equivalent circuit model being preferred for dynamic studies. Typically, the electrochemical and electric circuit models determine how battery models are classified; the other models are typically derived

from these models. To enhance the battery model, for instance, one can integrate current using Shepherd's equation. This model requires specific measurements to determine the battery's internal resistance.

The battery voltage during charge/discharge is given by (8).

$$V_b = E_b - RI_b \quad (8)$$

The voltage of the internal battery E_b is represented by (9)-(11).

$$E_b = E_o - k_B \frac{C}{i_t + 1C} i^* - K_B \frac{C}{C - i_t} i_t + \alpha(t); \text{ Charge } (i^* < 0) \quad (9)$$

$$E_b = E_o - k_B \frac{C}{C - i_t} i^* - K_B \frac{C}{C - i_t} i_t + \alpha(t); \text{ Discharge } (i^* < 0) \quad (10)$$

$$\alpha(t) = \int \frac{B}{t.(A.I_B - \alpha(t-1))} . dt \quad (11)$$

Where V_b is the battery voltage (V), R denotes the internal resistance, and I_b denotes the battery current. E_b denotes the no-load voltage (V).

2.4. PID controller

PID controller technology utilizes a feedback control loop to minimize disturbances impact on the system, guiding it towards the desired state and establishing clear relationships between system variables. The PID controller takes the error e_t at time t as input, which is the difference between the measured and reference values. The controller's output, the actuation α_t , represents the action to be applied to the system or plant. The actuation is determined by combining three terms: the proportional gain K_p multiplied by the error magnitude, the integral gain K_i multiplied by the integral of the error, and the derivative gain K_d multiplied by the derivative of the error. This creates a well-defined control signal that drives the system towards its desired state.

$$\alpha_t = K_p e_t + K_i \int_0^t e_t dt + K_d \frac{de_t}{dt} \quad (12)$$

The PID controller combines three terms to create the control signal: proportional gain K_p integral gain K_i and derivative gain K_d . K_p reduces steady-state error by responding to the present error. K_i addresses oscillations by considering past error accumulations. K_d anticipates future error changes and adds damping to prevent overshooting without affecting the steady-state error.

2.5. Seven level inverter

The pulse generation circuit design sets this topology apart from others, ensuring a unique pulse pattern to trigger switches at the precise moment. Switches S1, S2, and S3 must be unidirectional to prevent waveform distortion. The reduced number of switches makes the circuit more compact and user-friendly. The expression can be simplified as (13).

$$l = (2 * s - 3) = (2 * v - 1) \quad (13)$$

Where l is the voltage level, s is the number of switches, and v is the number of DC sources. Although 4 DC sources are used for the 7-level MLI, reduced switches lead to lower switching losses. Two switches are responsible for polarity reversal. Table 1 presents the switching scheme for this topology.

Table 1. Switching topology of 5 switch, 7 level inverter

S. No	S ₁	S ₂	S ₃	S ₄	S ₅	V _O
1	OFF	OFF	ON	OFF	ON	+V _{dc}
2	OFF	ON	OFF	OFF	ON	+2 V _{dc}
3	ON	OFF	OFF	OFF	ON	+3 V _{dc}
4	OFF	OFF	OFF	OFF	OFF	0
5	ON	OFF	OFF	ON	OFF	-V _{dc}
6	OFF	ON	OFF	ON	OFF	-2 V _{dc}
7	OFF	OFF	ON	ON	OFF	-3 V _{dc}

2.6. Transformer less UPQC

The TL-UPQC is connected to a low voltage (LV) distribution network at the point of common coupling (PCC) and consists of two half-bridge bi-directional voltage source converters (VSCs) sharing a common DC link, forming a topology with one shunt converter and one series converter. To minimize switching harmonics injected into the grid, a shunt filter capacitor acts as low impedance for high-frequency components introduced by the converter. The key features of the TL-UPQC topology include its transformer less design, resulting in higher efficiency and cost-effectiveness, low common-mode voltage achieved by clamping the potential difference between the AC and DC grounds, effective mitigation of harmonics from nonlinear loads, provision of reactive power to linear loads, fast dynamic response protecting critical loads from voltage flickering and disturbances, and the ability to control amplitude voltage variation for energy savings at the load bus.

In addition to its installation at a LV distribution network, the TL-UPQC can be optimized to perform the following functions: providing reactive power compensation for regulating the input grid voltage to loads connected at the PCC, enhancing the PCC voltage profile, and leading to an overall improvement in the upstream voltage quality. In a typical TL-UPQC system, the shunt converter is responsible for injecting current harmonics and reactive current i_p to compensate for the distorted current of the nonlinear load i_B connected to bus B. This shaping of the input current i_{PCC} ensures that it becomes sinusoidal and in phase with the PCC voltage. The grid current $i_G(t)$ carries the apparent power demand of the PCC load, represented by the PCC load current $i_A(t)$. Additionally, it carries the active power demand consumed by the load connected to the load bus, along with the necessary active power required to maintain the DC link voltage and compensate for converter losses. The proposed enhanced control methodology introduces an extra control degree of freedom, allowing the creation of a phase angle (θ) between V_{PCC} and I_{PCC} at the grid side. The expressions for active (P_{PCC}) and reactive (Q_{PCC}) power at the PCC can be defined as (14) and (15).

$$P_{PCC} = V_{PCC} I_{PCC} \cos \theta \quad (14)$$

$$Q_{PCC} = V_{PCC} I_{PCC} \sin \theta \quad (15)$$

θ is the phase angle by which the PCC current is displaced concerning its voltage.

To obtain the three-phase voltage reference signal for the series active power filter (APF), a phase-locked loop (PLL) is employed as shown in Figure 2.

$$U_a = \sin \omega t \quad (16)$$

$$U_b = \sin(\omega t - 120) \quad (17)$$

$$U_c = \sin(\omega t + 120) \quad (18)$$

$$V_{Labc}^* = V_m * U_{abc} \quad (19)$$

The TL-UPQC has the capability to operate in three distinct modes of reactive power compensation, which can be achieved by controlling the phase angle. In the power factor correction (PFC) mode, there is no need for reactive power compensation on the grid side. In the capacitive mode, the reactive power is injected into the grid, while in the inductive mode; the system absorbs reactive power from the grid. Prior to activating the grid reactive power compensation, the steady-state values are represented by I'_{PCC} , I'_G , and V'_{PCC} . The grid's active and reactive power transferred to the PCC bus can be expressed as (20) and (21).

$$P_g = \frac{V_G V_{PCC}}{Z_g} \cos(-\delta + \varphi_g) - \frac{V_{PCC}^2}{Z_g} \cos \varphi_g \quad (20)$$

$$Q_g = \frac{V_G V_{PCC}}{Z_g} \sin(-\delta + \varphi_g) - \frac{V_{PCC}^2}{Z_g} \cos \varphi_g \quad (21)$$

Here, the grid impedance Z_g is characterized by a displacement angle of φ_g . The active and reactive power of the linear load connected to the PCC is given as (22).

$$P_x = \frac{V_{PCC}^2}{Z_x} \cos \varphi_x : Q_x = \frac{V_{PCC}^2}{Z_x} \sin \varphi_x \quad (22)$$

The load impedance Z_x connected to the PCC, has a displacement angle φ_x . The TL-UPQC system provides harmonic compensation and active power control for non-linear loads, which is given by (23).

$$P_B = \frac{V_B^2}{R_B} \quad (23)$$

The TL-UPQC maintains a stable voltage V_B at the load bus by incorporating a fictitious resistance R_B .

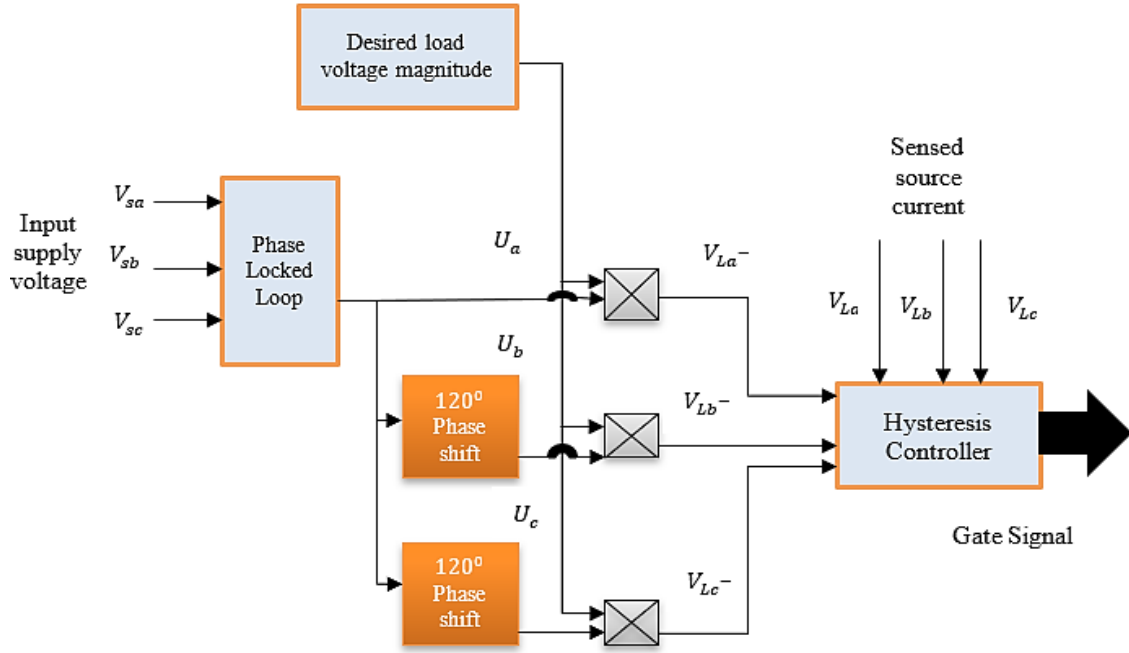


Figure 2. Control block diagram of series APF

Figure 3 shows the control block diagram of the shunt APF. In the TL-UPQC system, the power P_1 flowing through the shunt converter is utilized to charge the DC link capacitor and maintain a steady DC link voltage. This compensates for the power required by the series converter P_2 . The indicator of system stability is the constant value of the DC link voltage reached during steady-state operation. At equilibrium, the input power P_{PCC} matches the output power P_B . In short, the TL-UPQC achieves stability by balancing the power flow between the shunt and series converters, ensuring a constant DC link voltage.

$$\frac{V_G V_{PCC}}{Z_g} \cos(-\delta + \varphi_g) - \frac{V_{PCC}^2}{Z_g} \cos \varphi_g = \frac{V_B^2}{R_B} + \frac{V_{PCC}^2}{Z_A} \cos \varphi_A \quad (24)$$

The TL-UPQC system controls the voltage at the PCC by injecting or absorbing reactive power Q_{PCC} into or from the grid. To determine the required amount of reactive power for voltage regulation is given by (25).

$$Q_{PCC}(t) = \frac{V_G V_{PCC}}{Z_g} \sin(-\delta + \varphi_g) - \frac{V_{PCC}^2}{Z_g} \sin \varphi_g - \frac{V_{PCC}^2}{Z_A} \sin \varphi_A \quad (25)$$

The shunt active power filter (APF) serves to mitigate current harmonics and regulate the DC link voltage at a constant level. It operates similarly to the series APF but with the additional role of monitoring and comparing the actual DC link voltage with the desired reference level. The resulting error signal is used in a PID controller to generate a reference source current signal, which in turn is multiplied by the error signal.

$$I_{sabc}^* = I_m^* U_{abc} \quad (26)$$

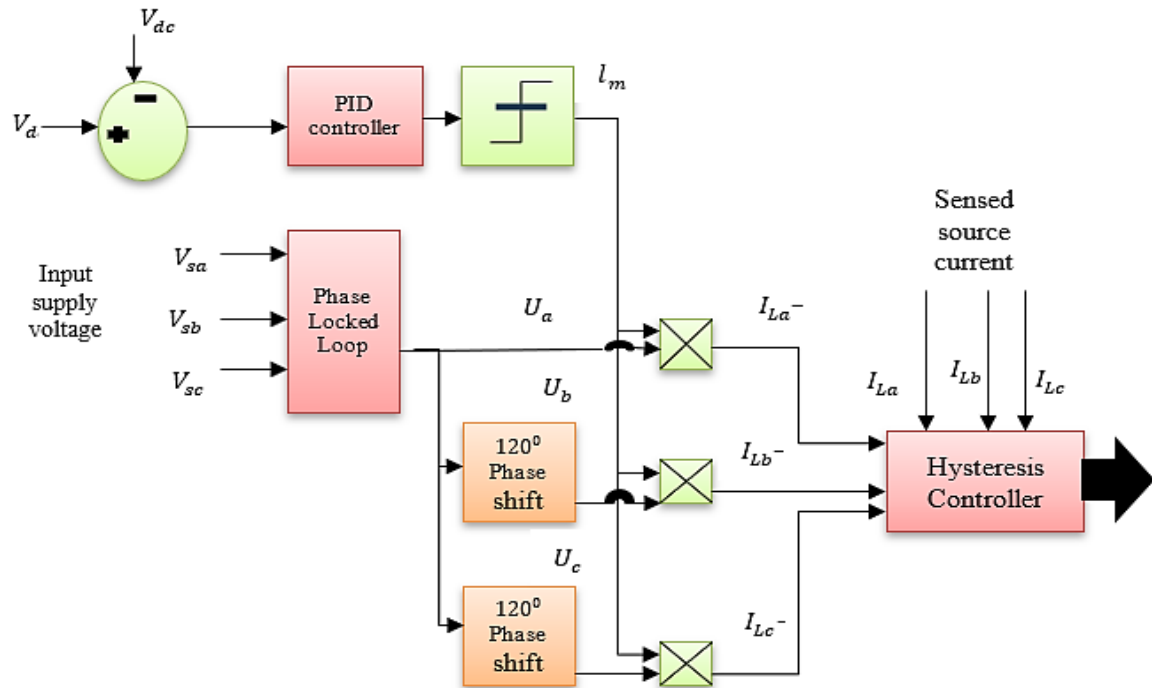


Figure 3. Control block diagram of shunt APF

3. RESULTS AND DISCUSSION

The HBEO algorithm was employed to optimize the PID controller in the proposed model. The performance of the HBEO-optimized PID controller was evaluated under various operating conditions, including different solar irradiance levels and temperature variations. The simulation outputs are the PV output, battery output, sag, swell, fluctuation mitigation, and THD.

3.1. Analysis of PV characteristics

Constant solar radiance, variable solar irradiance, and variable temperature are some of the PV characteristics of a PV system. Figure 4 provides the PV characteristics with variations in solar irradiance and temperature. When analyzing PV characteristics in a PV system a steady supply of solar energy, or sunlight strength, is presumed or retained is referred to as constant solar radiance. Time is compared with voltage, current, and power. When analyzing a photovoltaic system's effectiveness or predicting its future behavior, an average or steady solar radiation level is frequently used as a point of comparison. Figure 4(a) represents the constant solar radiance. The term "variable solar irradiance" describes how the amount of UV rays that a specific place receives varies as time passes. The amount of energy per unit area is known as solar irradiance. Regarding renewable energy sources such as solar power plants, variable sun irradiance is an essential factor in the creation, assessment of efficiency, and improvement processes. Figure 4(b) depicts the variable solar irradiance. The term "variable temperature" in photovoltaic (PV) characteristics describes the temperature variations that occur while photovoltaic cells or solar panel assemblies are in use. Temperature has a significant impact on several elements of PV features and is a major factor impacting PV system efficiency. Voltage, current, and power are made a comparison with the time in a PV characteristic in the PV system. Figure 4(c) shows the variable temperature.

3.2. Analysis of battery characteristics

The following graph contained in Figure 5 shows the voltage, current, and power placed on the y-axis, and the curves are measured under the different temperatures on the x-axis. The current capacity to nominal capacity ratio is typically used to calculate a battery's SOC characterized by several criteria that specify their actions, their limits, and their effectiveness. The batteries' comparatively linear gradient, as can be shown, makes it easy to calculate the related SoC value fairly accurately from the observed voltage. From 0.3% to 0.05%, SOC increases linearly as charging continues. After the battery SOC hits 100 W, the charging current is gradually raised from 0.2 A to 0.3 A even though the battery voltage remains constant at 280 V.

3.3. Analysis of DC link voltage

The voltage range is indicated on the y-axis and the time (sec) is represented on the x-axis as shown in Figure 6. This DC circuit is necessary to offer a steady DC voltage and prevent fluctuations as the inverter occasionally requires a large current to convert the energy produced by solar PV panels into a format suitable for connecting to the grid or other applications. Therefore, it is demonstrated that a steady voltage of 250 V is reached within 0.25 seconds, allowing for efficient energy storage and high-frequency switching of currents.

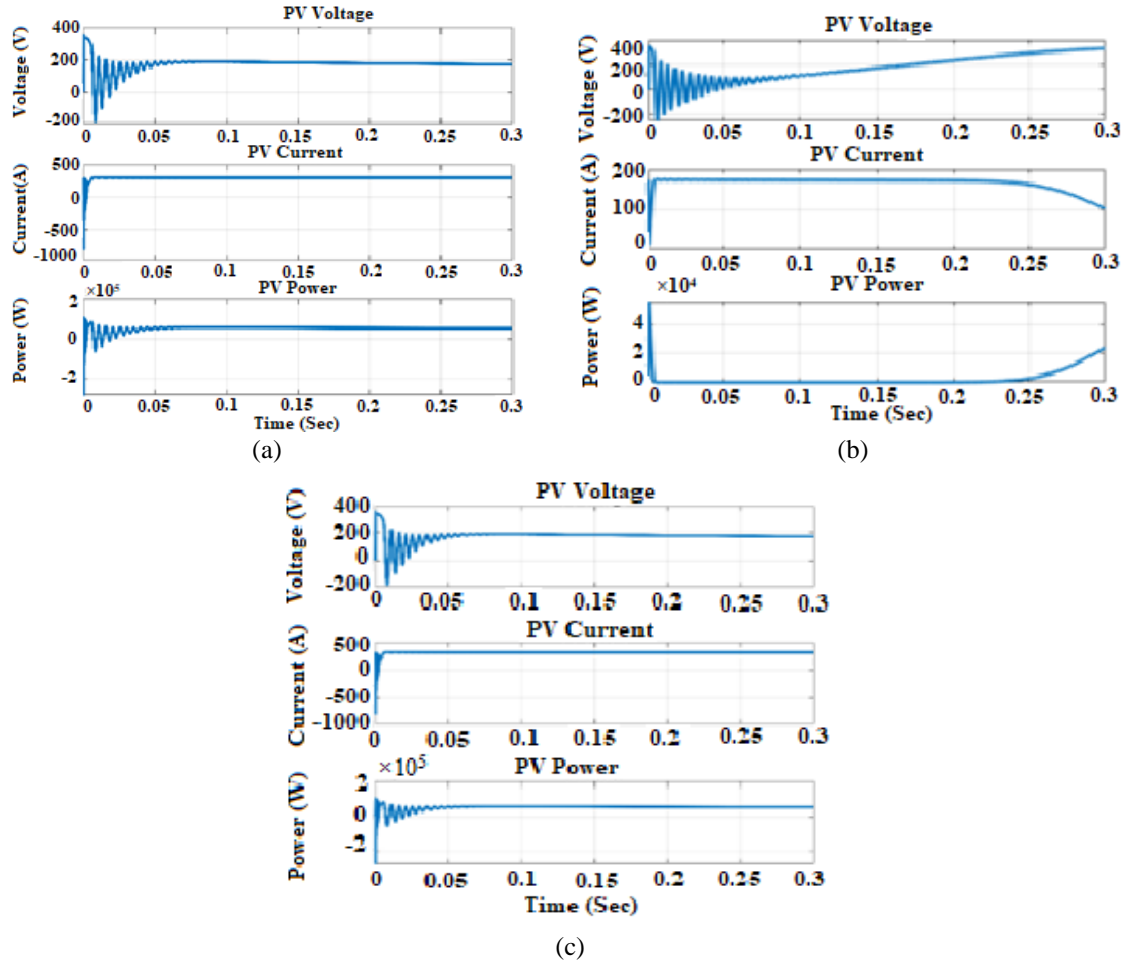


Figure 4. PV characteristics of (a) constant solar radiance, (b) variable solar irradiance, and (c) variable temperature

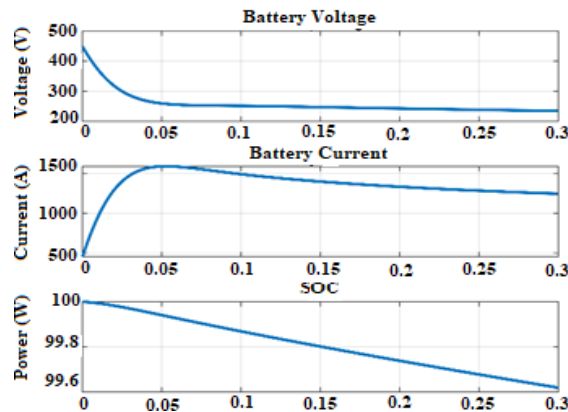


Figure 5. Battery characteristics

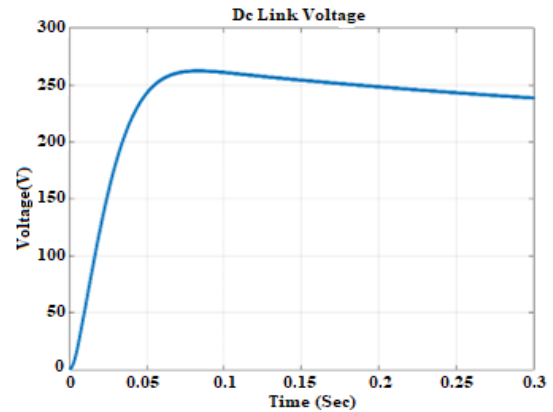


Figure 6. DC link voltage

3.4. Analysis of seven-level voltage output

In a photovoltaic (PV) system, the term "seven-level voltage output" usually implies the total quantity of levels of voltage that are included in the waveform that comes out of the transformer. Establishing a multilayer output voltage is a strategy that will enhance the efficiency of the produced AC power and eliminate distortion caused by harmonics in the setting of power circuits and processors utilized in photovoltaic systems. The output of the seven-level inverter is shown in Figure 7. The seven levels are 0, ± 10 V, ± 20 V, and ± 30 V.

3.5. Analysis of source real and reactive power

Terminology related to the electricity produced and supplied by the system in question includes real power, often referred to as active power and reactive power about the situation of photovoltaic (PV) systems and their features. The real power in a system of electricity is represented by the letter P and represents the real source of energy that does work. It is the energy that is transformed into functional electric or mechanical activity. Real power in the context of a photovoltaic system is the actual energy output that is transformed into electrical power that can be used. The relationship between voltage (V), current (I), and real power (P) is given. The power that isn't doing any work but is required for the creation and upkeep of electromagnetic waves in the electrical grid is known as reactive power, represented by the letter Q. The unit of measurement is VAR, or volt-amperes reactive. The source side of real and reactive power is shown in Figure 8.

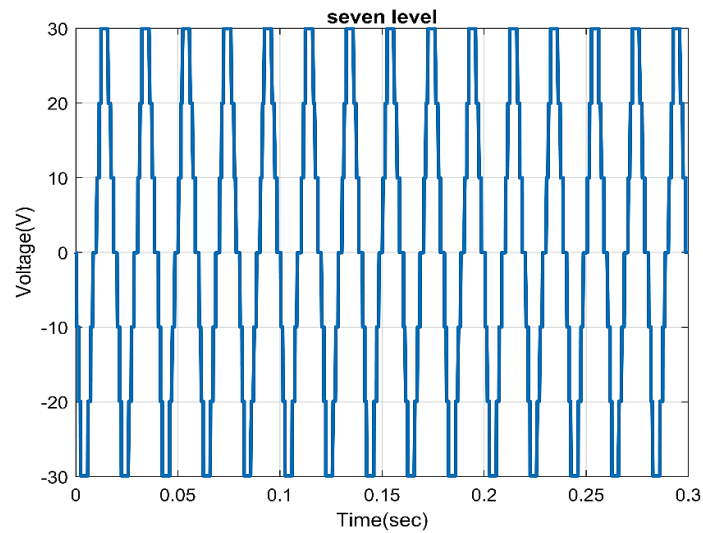


Figure 7. Seven-level voltage output

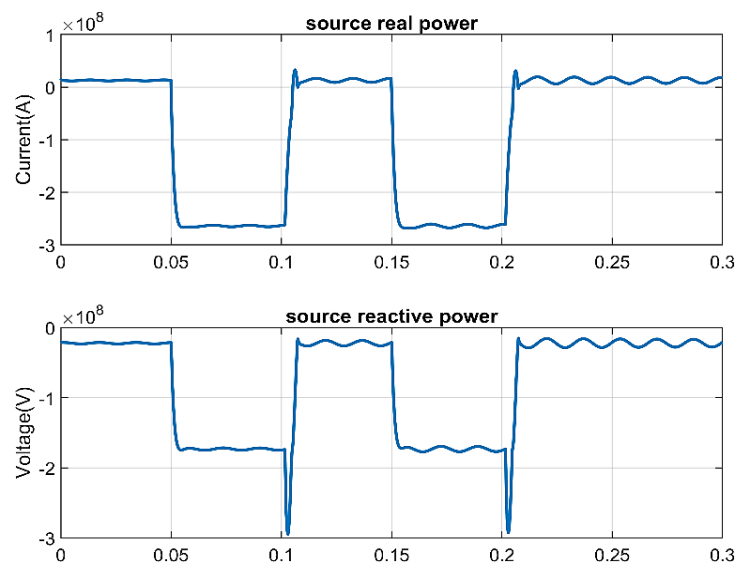


Figure 8. Source real and reactive power

3.6. Analysis of sag, swell, and fluctuation mitigation

In Figure 9, the fault occurs at 0.05 s and the current is injected at 0.05 s to 0.1 s to mitigate the sag, swell, and fluctuation. When referring to different power reliability problems in electrical systems, particularly those linked to photovoltaic (PV) systems, the phrases sag, swell, and fluctuation are utilized. These concepts describe brief variations in voltage that may have an impact on the dependability and efficiency of electrical devices. A brief drop in the level of voltage under the normal voltage is referred to as a sag, often called a voltage dip. Some things, such as heavy loads initiating, electrical shorts, or other abrupt shifts in the electrical grid, can result in sags as shown in Figure 9(a). A brief rise in voltage over the voltage that is normal is called a swell. Phenomena like load shifting, abrupt disconnections of heavy loads, or modifications to the network can all result in swells as shown in Figure 9(b). Fast and frequent changes in the level of voltage are referred to as voltage fluctuation. Heavy stress operations, modifications to the system setup, and sporadic malfunctions can all cause fluctuations that can be represented in Figure 9(c).

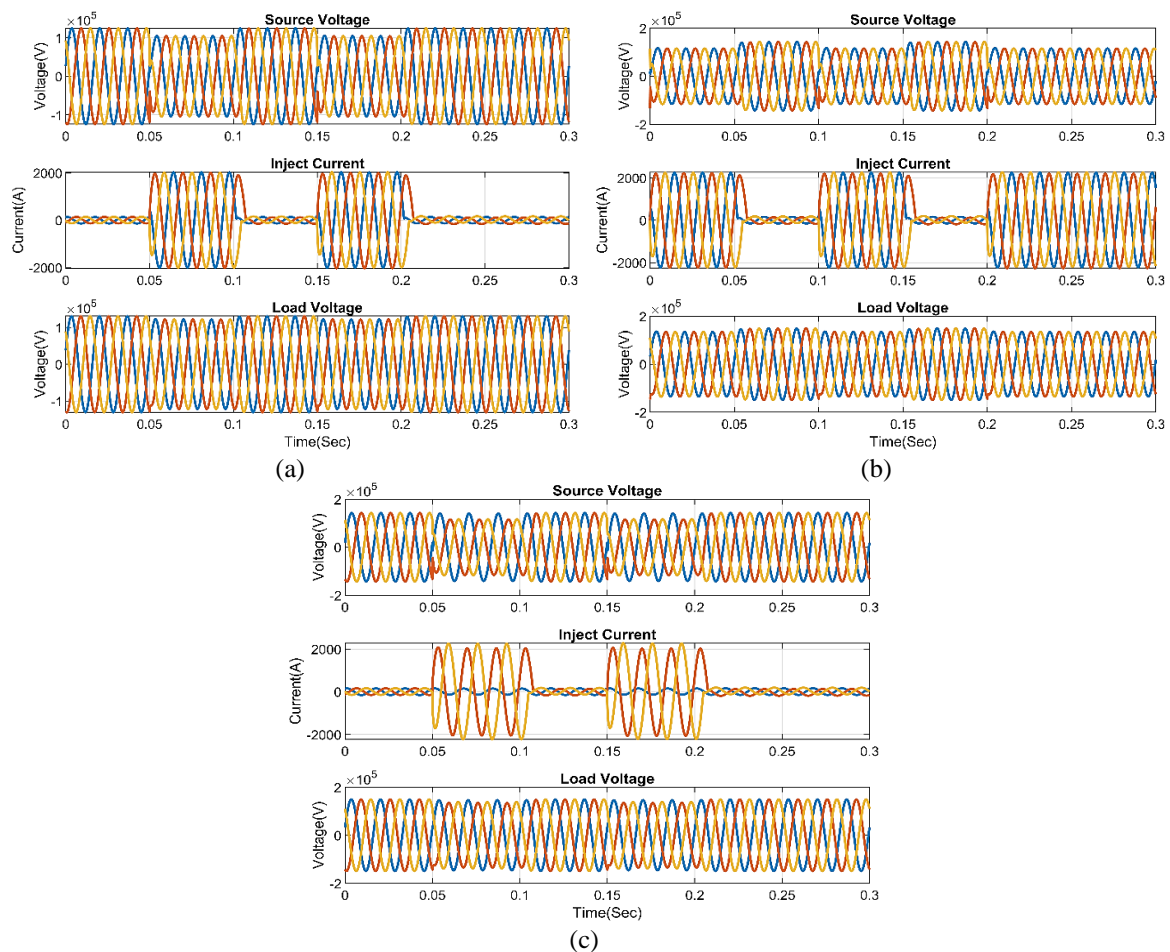


Figure 9. Analysis of (a) sag, (b) swell, and (c) fluctuation mitigation

3.7. Comparison of sag, swell, and fluctuation

Figure 10 shows a comparative study with existing optimization techniques such as PSO, GA, and moth flame optimization (MFO) to achieve optimum power quality (PQ) in a hybrid power system integrating battery and PV. Figure 10(a) shows the sag comparison of the proposed HBEO with the other existing optimization methods. The proposed method achieves a reduced output voltage of 3.8 KV compared with others that attained better efficiency. The voltage reduction can be obtained during the swell comparison in the proposed method achieves 14 V as more convergence when compared to the other optimization techniques that can be shown in Figure 10(b). Similarly, the output generated in the voltage reduced through fluctuation on the proposed method achieves a 15 V, when compared with other existing research as shown in Figure 10(c), and also attains better optimal integrity.

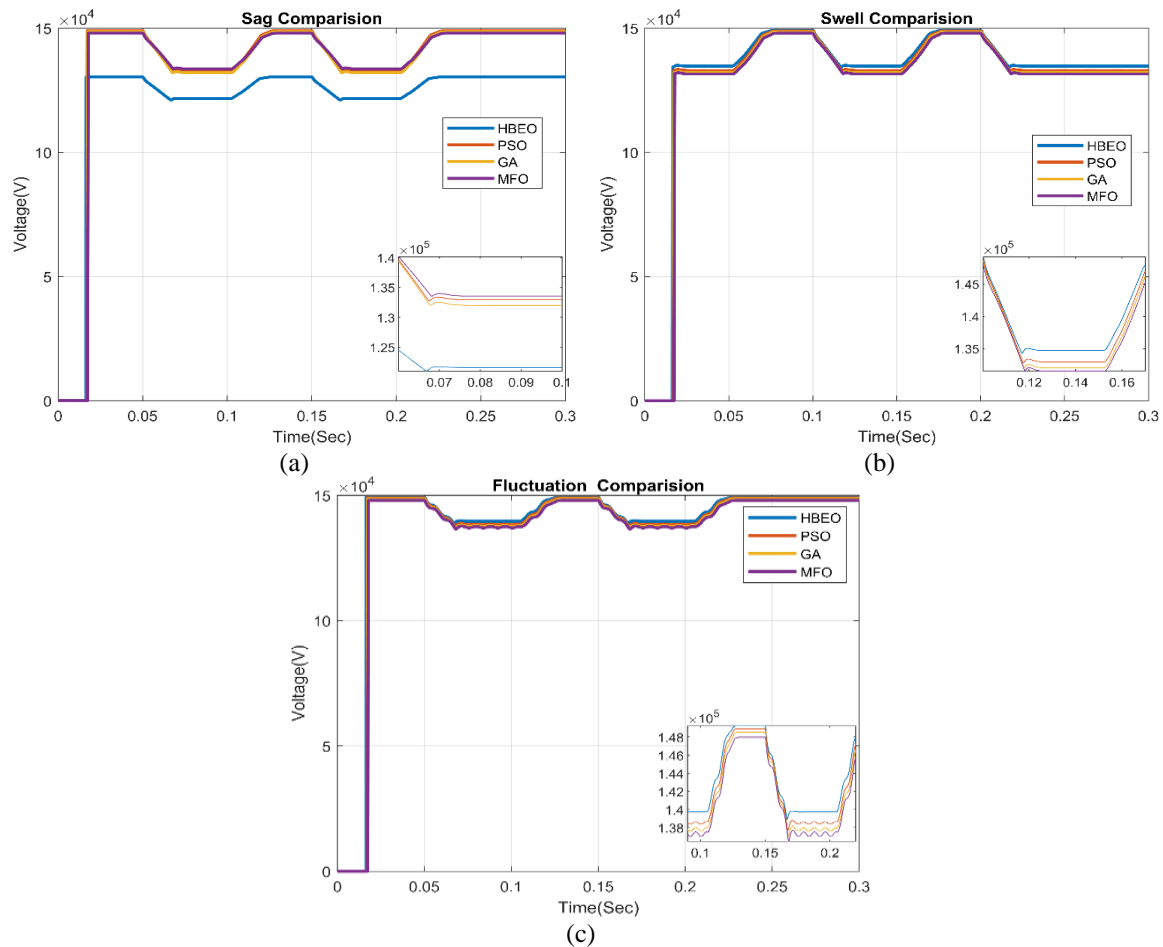


Figure 10. Comparison of (a) sag, (b) swell, and (c) fluctuation

3.8. Analysis of THD

The power method's total harmonic distortion (THD) can be reduced by using particle swarm optimization (PSO). PSO is a heuristic optimization technique, and the particulars of the optimization challenge as well as variable adjustment can affect how well it performs. It is essential to verify the outcomes, either through models or tests, to ascertain the efficacy of the improved settings in reducing total harmonic distortion within the real power system. Figure 11(a) shows the PSO.

Under the framework of a photovoltaic (PV) system, a genetic algorithm (GA) is a computer-optimizing method that draws inspiration from the laws of biological selection and heredity. Evolving algorithms that are employed for approximating responses to enhancement and search-related issues include genetic algorithms. Utilizing a genetic algorithm in the framework of a PV system may have the objective of optimizing particular system setups or characteristics to improve affordability, execution, or reliability. Figure 11(b) depicts the GA concerning photovoltaic (PV) systems, the mayfly optimization algorithm is particularly useful in tackling the problem of precise identification of parameters for PV cells. Figure 11(c) shows the MFO. The THD of PSO is 14.7803, GA is 17.0865, MFO is 18.9207, and the proposed HBEO model is 0.0080733. This shows that the proposed method has superior performance when compared with other methods which can be depicted in Figure 11(d).

3.9. Comparison of THD

The THD is compared with the PID, PD, Pi, and P. Proportional-integral-derivative, or PID, controllers are a kind of control system with feedback that is extensively utilized in commercial and technical settings, particularly photovoltaic systems. A PID controller is used for regulating the performance of a system by measuring the discrepancy between the real result and an ideal goal. One kind of control system with feedback that is frequently utilized in the setting of a photovoltaic system is the P controller, also known as the proportional controller. The P controller is frequently a component of the control plan used in PV systems to regulate the generated electricity or voltage to attain the intended efficiency and guarantee system functionality.

In the framework of photovoltaic systems, a PI controller, also known as a proportional-integral controller, is a kind of feedback system for control. The proportional controller is extended by the PI controller, which adds an extra fundamental phrase to enhance system efficiency, particularly in removing steady-state faults. The derivative part and the term for proportionality are integrated into a PID controller to enhance the reliability and performance of the overall system. THD comparison with P, PI, PD, and PID controllers are represented in Figure 12.

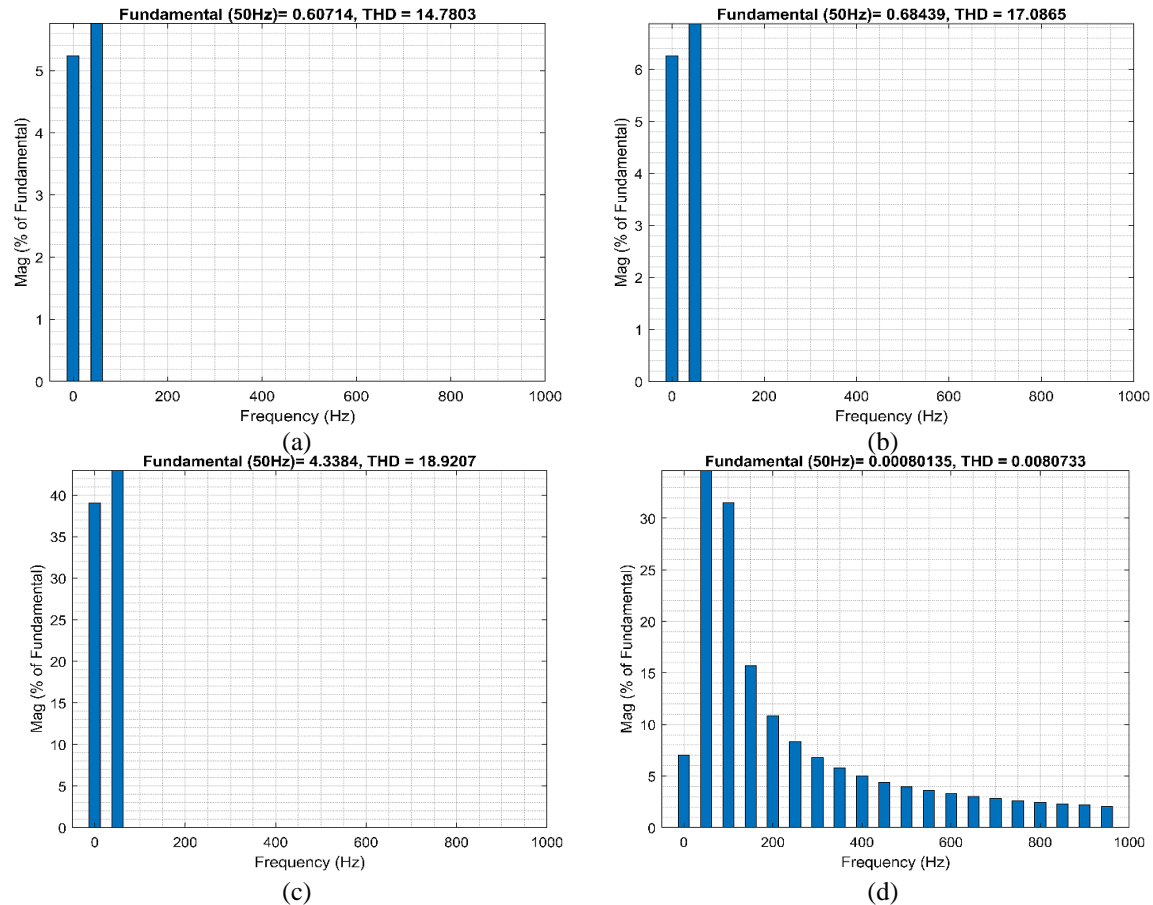


Figure 11. THD analysis: (a) PSO, (b) GA, (c) MFO, and (d) proposed HBEO

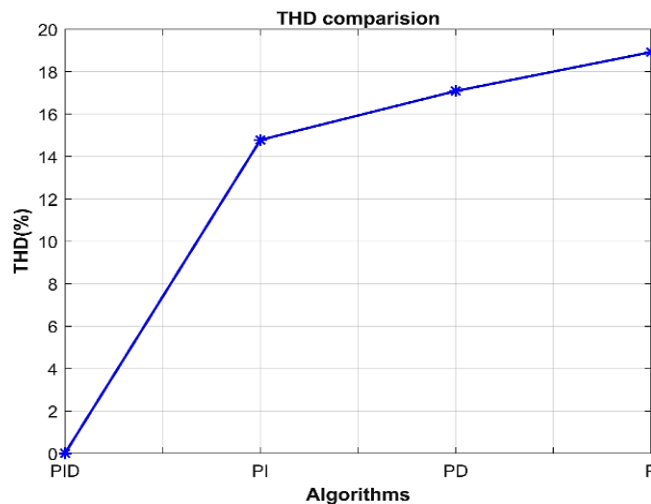


Figure 12. THD comparison with P, PI, PD, and PID controllers

4. CONCLUSION

This research introduces an effective transformer less seven-level inverter with optimized PID and buck-boost controllers for grid-connected PV systems. The proposed model aims to achieve optimum power quality (PQ) in a hybrid power system incorporating battery and PV integration. To achieve this, a unified power quality conditioner with active and reactive power (UPQC-PQ) is adapted with a PID controller optimized using the HBEO algorithm. The optimized PID controller enhances system stability, responsiveness, and reduces ITAE values. Trapezoidal pulse width modulation (PWM) is employed to reduce total harmonic distortion (THD) in the output voltage. The model's 7-level multilevel inverter design with minimal switch usage ensures reduced switching losses. Implementation and verification are conducted under diverse temperature and solar irradiance conditions, demonstrating its effectiveness. Comparative analysis with PSO, GA, and MO showcases the superiority of the HBEO algorithm. The proposed model, simulated on MATLAB/Simulink, provides an efficient solution for enhancing power quality in grid-connected PV systems.




REFERENCES

- [1] J. R. Rodriguez *et al.*, "A single-loop and current-sensorless control for on-grid seven-level photovoltaic microinverter," *IET Power Electronics*, vol. 16, no. 6, pp. 905–916, May 2023, doi: 10.1049/pel2.12436.
- [2] B. Aljafari, A. K. Loganathan, I. Vairavasundaram, S. Ramachadran, and A. P. Nagarajan, "Analysis of a Photovoltaic System Based on a Highly Efficient Single-Phase Transformerless Inverter," *Energies*, vol. 15, no. 17, p. 6145, Aug. 2022, doi: 10.3390/en15176145.
- [3] B. Sabir, S.-D. Lu, H.-D. Liu, C.-H. Lin, A. Sarwar, and L.-Y. Huang, "A Novel Isolated Intelligent Adjustable Buck-Boost Converter with Hill Climbing MPPT Algorithm for Solar Power Systems," *Processes*, vol. 11, no. 4, p. 1010, Mar. 2023, doi: 10.3390/pr11041010.
- [4] G. Goswami and P. K. Goswami, "Power quality improvement at nonlinear loads using transformer-less shunt active power filter with adaptive neural fuzzy interface system supervised PID controllers," *International Transactions on Electrical Energy Systems*, vol. 30, no. 7, Jul. 2020, doi: 10.1002/2050-7038.12415.
- [5] A. I. M. Ali, M. A. Sayed, and A. A. S. Mohamed, "Seven-level inverter with reduced switches for pv system supporting home-grid and EV charger," *Energies*, vol. 14, no. 9, p. 2718, May 2021, doi: 10.3390/en14092718.
- [6] A. K. Yadav, K. Gopakumar, R. Krishna Raj, L. Umanand, S. Bhattacharya, and W. Jarzyna, "A Hybrid 7-Level Inverter Using Low-Voltage Devices and Operation with Single DC-Link," *IEEE Transactions on Power Electronics*, vol. 34, no. 10, pp. 9844–9853, Oct. 2019, doi: 10.1109/TPEL.2018.2890371.
- [7] B. Saleh *et al.*, "Design of PID Controller with Grid Connected Hybrid Renewable Energy System Using Optimization Algorithms," *Journal of Electrical Engineering and Technology*, vol. 16, no. 6, pp. 3219–3233, Nov. 2021, doi: 10.1007/s42835-021-00804-7.
- [8] G. Goswami and P. K. Goswami, "A design analysis and implementation of PI, PID and fuzzy supervised shunt APF at nonlinear load application to improve power quality and system reliability," *International Journal of System Assurance Engineering and Management*, vol. 12, no. 6, pp. 1247–1261, Dec. 2021, doi: 10.1007/s13198-021-01179-8.
- [9] H. Azeem, S. Yellasi, V. Jammala, B. S. Naik, and A. K. Panda, "A Fuzzy Logic Based Switching Methodology for a Cascaded H-Bridge Multi-Level Inverter," *IEEE Transactions on Power Electronics*, vol. 34, no. 10, pp. 9360–9364, Oct. 2019, doi: 10.1109/TPEL.2019.2907226.
- [10] K. B. Kumar, A. Bhanuchandar, and C. Mahesh, "A Novel Control Scheme for Symmetric Seven Level Reduced Device Count Multi-Level DC Link (MLDCL) Inverter," in *2021 International Conference on Sustainable Energy and Future Electric Transportation (SEFET)*, Jan. 2021, pp. 1–4, doi: 10.1109/SeFet48154.2021.9375714.
- [11] L. Meng *et al.*, "Control Strategy of Single-Phase UPQC for Suppressing the Influences of Low-Frequency DC-Link Voltage Ripple," *IEEE Transactions on Power Electronics*, pp. 1–1, 2021, doi: 10.1109/TPEL.2021.3106049.
- [12] M. A. Khan, A. Haque, and V. S. B. Kurukuru, "Performance assessment of stand-alone transformerless inverters," *International Transactions on Electrical Energy Systems*, vol. 30, no. 1, Jan. 2020, doi: 10.1002/2050-7038.12156.
- [13] M. A. Mansor, K. Hasan, M. M. Othman, S. Z. B. M. Noor, and I. Musirin, "Construction and Performance Investigation of Three-Phase Solar PV and Battery Energy Storage System Integrated UPQC," *IEEE Access*, vol. 8, pp. 103511–103538, 2020, doi: 10.1109/ACCESS.2020.2997056.
- [14] M. Biswas, S. P. Biswas, M. R. Islam, M. A. Rahman, K. M. Muttaqi, and S. M. Mueen, "A New Transformer-Less Single-Phase Photovoltaic Inverter to Improve the Performance of Grid-Connected Solar Photovoltaic Systems," *Energies*, vol. 15, no. 22, p. 8398, Nov. 2022, doi: 10.3390/en15228398.
- [15] N. Gao *et al.*, "MOSFET-Switch-Based Transformerless Single-Phase Grid-Tied Inverter for PV Systems," *IEEE Journal of Emerging and Selected Topics in Power Electronics*, vol. 10, no. 4, pp. 3830–3839, Aug. 2022, doi: 10.1109/JESTPE.2021.3064587.
- [16] N. V. Kurdkandi, M. Ghavipanjeh Marangalu, T. Hemmati, S. H. Hosseini, O. Husev, and A. Khsokhbar-sadigh, "Single-Phase Two-Stage Transformerless Grid-Connected Inverter For Photovoltaic Applications," in *2021 12th Power Electronics, Drive Systems, and Technologies Conference (PEDSTC)*, Feb. 2021, pp. 1–5, doi: 10.1109/PEDSTC52094.2021.9405959.
- [17] P. C. Sahu, R. C. Prusty, and S. Panda, "Frequency regulation of an electric vehicle-operated micro-grid under WOA-tuned fuzzy cascade controller," *International Journal of Ambient Energy*, vol. 43, no. 1, pp. 2900–2911, Dec. 2022, doi: 10.1080/01430750.2020.1783358.
- [18] P. K. Chillappagari, K. Nagaraj, and M. R. Airineni, "Open-circuit fault resilient ability multi level inverter with reduced switch count for off grid applications," *International Journal of Electrical and Computer Engineering*, vol. 12, no. 3, pp. 2353–2362, Jun. 2022, doi: 10.11591/ijece.v12i3.pp2353-2362.
- [19] R. Abdalaal and C. N. M. Ho, "System Modeling and Stability Analysis of Single-Phase Transformerless UPQC Integrated Input Grid Voltage Regulation," *IEEE Journal of Emerging and Selected Topics in Industrial Electronics*, vol. 3, no. 3, pp. 670–682, Jul. 2022, doi: 10.1109/JESTIE.2021.3091395.
- [20] S. A. Zaid, H. Albalawi, H. AbdelMeguid, T. A. Alhmiedat, and A. Bakeer, "Performance Improvement of H8 Transformerless Grid-Tied Inverter Using Model Predictive Control Considering a Weak Grid," *Processes*, vol. 10, no. 7, p. 1243, Jun. 2022, doi: 10.3390/pr10071243.




- [21] S. Padmanaban, N. Priyadarshi, M. S. Bhaskar, J. B. Holm-Nielsen, V. K. Ramachandaramurthy, and E. Hossain, "A Hybrid ANFIS-ABC Based MPPT Controller for PV System with Anti-Islanding Grid Protection: Experimental Realization," *IEEE Access*, vol. 7, pp. 103377–103389, 2019, doi: 10.1109/ACCESS.2019.2931547.
- [22] S. Poongothai and S. Srinath, "Power quality enhancement in solar power with grid connected system using UPQC," *Microprocessors and Microsystems*, vol. 79, p. 103300, Nov. 2020, doi: 10.1016/j.micpro.2020.103300.
- [23] S. P. Bihari and P. K. Sadhu, "Design analysis of high level inverter with EANFIS controller for grid connected PV system," *Analog Integrated Circuits and Signal Processing*, vol. 103, no. 3, pp. 411–424, Jun. 2020, doi: 10.1007/s10470-019-01578-9.
- [24] K. J. Sinu and G. Ranganathan, "A PV FED three phase switched Z-source multi level inverter for induction motor drives," *Indonesian Journal of Electrical Engineering and Computer Science*, vol. 9, no. 1, pp. 24–28, Jan. 2018, doi: 10.11591/ijeecs.v9.i1.pp24-28.
- [25] V. Burlaka, S. Gulakov, and S. Podnebennaya, "Low-Cost Transformerless Grid-Tie Inverter For Photovoltaic System," in *2019 IEEE 6th International Conference on Energy Smart Systems (ESS)*, Apr. 2019, pp. 334–338, doi: 10.1109/ESS.2019.8764200.

BIOGRAPHIES OF AUTHORS






B. Mohan Rao    has research scholar at the Department of Electrical Engineering, University College of Engineering, Osmania University, Hyderabad, India. He received master of technology (M.Tech.) in power electronics (PE) from Laqshya Institute of Technology and Sciences, Khammam, India in 2015, and he received bachelor of technology (B.Tech.) in electrical and electronics engineering, Aurora's Technological and Research Institute, Hyderabad, India in 2012. He can be contacted at email: bodamohan1@osmania.ac.in or bodamohan1@gmail.com.



Mohammad Haseeb Khan    received his B.Tech. (EEE) from Kakatiya University in the year 1999, M.Tech. (power electronics) and Ph.D. (EEE) in the years 2003 and 2012 respectively from Jawaharlal Nehru Technological University, Hyderabad. He has more than 23 years of teaching experience and has published about 30 papers in national and international conferences and journals. Currently, he is working as a professor and head, of the Electrical Engineering Department, at Muffakham Jah College of Engineering and Technology, Hyderabad. His research areas include power electronics and its applications, electric drives, intelligent systems, and power quality. He can be contacted at email: haseebkhaneed@mjclege.ac.in.



B. Mangu    received the B.E. and M.E. degrees from the University College of Engineering, Osmania University, Hyderabad, India, in 2000 and 2005, and the Ph.D. degree from the Department of Electrical Engineering, IIT Bombay, Mumbai, India. He has been with the Department of Electrical Engineering, University College of Engineering, Osmania University, since 2001, where he is also a professor. His current research interests include the design of converters for the integration of renewable sources. He can be contacted at email: bmanguou@gmail.com.